

## Multiparticle Cumulant Mapping for Coulomb Explosion Imaging

Chuan Cheng<sup>1</sup>, Leszek J. Frasiniski<sup>2</sup>, Gönenç Moğol<sup>1</sup>, Felix Allum<sup>3,4,5</sup>, Andrew J. Howard<sup>4,6</sup>, Daniel Rolles<sup>7</sup>, Philip H. Bucksbaum<sup>4,5</sup>, Mark Brouard<sup>3</sup>, Ruaridh Forbes<sup>4,5</sup>, and Thomas Weinacht<sup>1</sup>

<sup>1</sup>*Department of Physics and Astronomy, Stony Brook University, Stony Brook, New York 11794, USA*

<sup>2</sup>*Department of Physics, Imperial College London, Prince Consort Road, London SW7 2AZ, United Kingdom*


<sup>3</sup>*Chemistry Research Laboratory, Department of Chemistry, University of Oxford, Oxford OX1 3TA, United Kingdom*

<sup>4</sup>*Stanford PULSE Institute, SLAC National Accelerator Laboratory, Menlo Park, California 94025, USA*

<sup>5</sup>*Linac Coherent Light Source, SLAC National Accelerator Laboratory, Menlo Park, California 94025, USA*

<sup>6</sup>*Department of Applied Physics, Stanford University, Stanford, California 94305, USA*

<sup>7</sup>*J.R. Macdonald Laboratory, Department of Physics, Kansas State University, Manhattan, Kansas 66506, USA*

 (Received 28 October 2022; accepted 2 February 2023; published 2 March 2023)

We extend covariance velocity map ion imaging to four particles, establishing cumulant mapping and allowing for measurements that provide insights usually associated with coincidence detection, but at much higher count rates. Without correction, a fourfold covariance analysis is contaminated by the pairwise correlations of uncorrelated events, but we have addressed this with the calculation of a full cumulant, which subtracts pairwise correlations. We demonstrate the approach on the four-body breakup of formaldehyde following strong field multiple ionization in few-cycle laser pulses. We compare Coulomb explosion imaging for two different pulse durations (30 and 6 fs), highlighting the dynamics that can take place on ultrafast timescales. These results have important implications for Coulomb explosion imaging as a tool for studying ultrafast structural changes in molecules, a capability that is especially desirable for high-count-rate x-ray free-electron laser experiments.

DOI: [10.1103/PhysRevLett.130.093001](https://doi.org/10.1103/PhysRevLett.130.093001)

Multiparticle coincidence measurements have provided a remarkable window into the structure and dynamics of small molecules [1–10]. In particular, Coulomb explosion imaging (CEI) can provide insight into many structural changes occurring in photoexcited molecules including isomerization [11–13], dissociation [14–21], roaming [22–25], hydrogen migration [26,27], and bond cleavage [28]. CEI relies on multiple ionization of the target molecule, followed by a measurement of the relative momenta of the resultant ionic fragments, from which structural information can be inferred. Particularly for larger molecules, a high degree of ionization and fragmentation of the target must be achieved, and many fragments must be detected in order to extract meaningful structural information. This technique is of great interest, because it can provide time-resolved information on molecular structure in the recoil frame. Recently, both strong field ionization and x-ray multiphoton ionization-induced CEI have yielded promising results in studies that make use of multiparticle correlations [12,19,22,29–31].

While coincidence measurements have been extremely useful for establishing multiparticle correlations, the low event rates required to avoid false coincidences make the repeated measurements necessary for tracking time-dependent structural changes challenging [7]. Fortunately, in the high-event-rate regime, covariance analysis that measures linear correlation among particles has been

developed and widely used for two-body and three-body correlations [32–34]. Some tabletop and free-electron laser (FEL)-based experiments have already incorporated this statistical analysis technique [7,16,19,34–37]. While experiments at FEL beam lines have drawn a lot of attention, FEL pulses are subject to large temporal and spectral fluctuations. These can be dealt with using more extended techniques, such as partial and contingent covariance [38–40]. However, covariance measurements have not yet been established in four-or-more-body relationships, because four-body and higher covariance is qualitatively different from two- and three-body [39,41]. This can be seen by evaluating the expressions for collective correlations among a few fragments:

$$\chi_n(A, B, \dots) = \langle (N_A - \langle N_A \rangle)(N_B - \langle N_B \rangle)(\dots) \rangle, \quad (1)$$

where  $\chi_n$  is the  $n$ -fold covariance and  $N_A$  denotes the number of fragments of species  $A$  generated in a given measurement. The brackets  $\langle \dots \rangle$  represent an expectation value. If one assumes that the number of fragments follows a Poisson distribution, then one can show that [41,42]

$$\begin{aligned} \chi_2(A, B) &= \langle N_{AB} \rangle, \\ \chi_3(A, B, C) &= \langle N_{ABC} \rangle, \\ \chi_4(A, B, C, D) &= \langle N_{ABCD} \rangle + \sum^3 \langle N_{AB} \rangle \langle N_{CD} \rangle. \end{aligned} \quad (2)$$

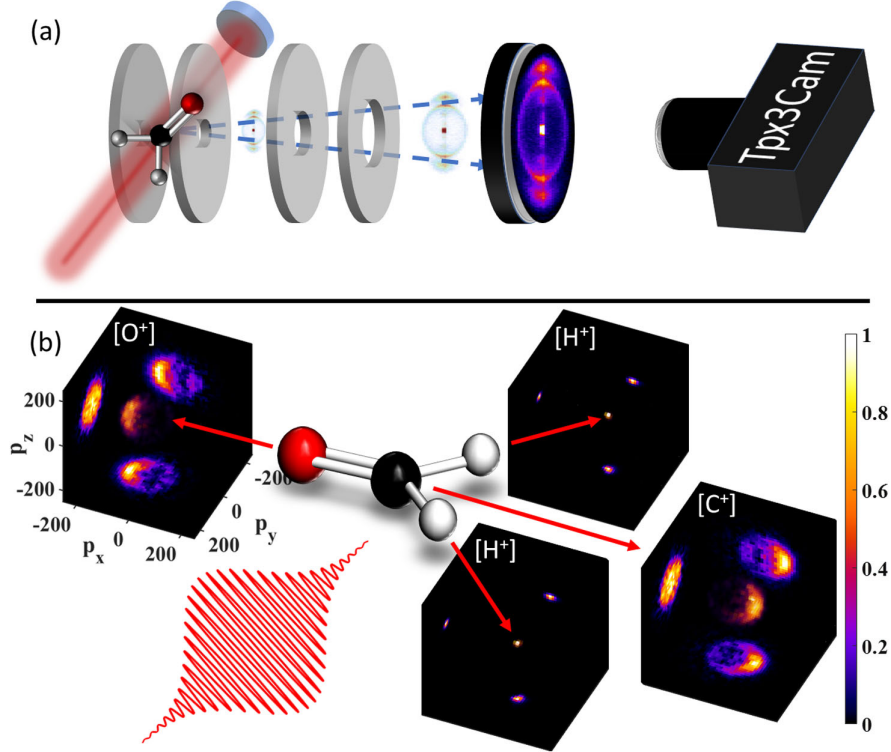


FIG. 1. Diagram of the experimental setup and demonstration of recoil frame reconstruction using the fourfold cumulant:  $\chi_4(\text{H}^+, \text{H}^+, \text{C}^+, \text{O}^+)$ . (a) shows the VMI assembly, where ionization happens and fragments are accelerated toward microchannel plates (MCP) and phosphor. The phosphor is imaged on the Tpx3Cam camera and centroided to obtain 3D ion momentum. (b) shows fourfold momentum-resolved covariance of fragments from the quadruple ionization of  $\text{CH}_2\text{O}$  using a 30-fs, 800-nm,  $240 \text{ TW}/\text{cm}^2$  linearly polarized pulse. The positive  $x$  axis and  $xy$  plane are defined by the momenta of the two protons, with the positive  $x$  axis defined by their bisector. Momentum units are  $\hbar/a_0$ . A ball-and-stick model of the molecule is included to illustrate the relationship between the correlated momenta and the recoil frame.

Here, the sum is over the three ways of pairing the four variables.  $N_{AB}$  (similar for  $N_{ABC}$ , etc.) denotes the number of events in which fragments  $A$  and  $B$  are generated together (e.g.,  $\text{CD}_2\text{O}^{2+} \rightarrow \text{CD}_2^+ + \text{O}^+$ ).

Starting from the fourth-order covariance,  $\chi_n$  will have contributions from pairwise correlations  $\langle N_{AB} \rangle \dots$  that are independent or separate from the full  $N$ -body correlations of interest. This will lead to a nonzero correlation value even in the absence of collective correlation among all  $N$  fragments [39]. With a small correction, the covariance formula can be modified to capture only the full four-body correlations, which is equivalent to a fourfold cumulant [41]:

$$\chi_4 = \chi_4 - \sum^3 \chi_2(A, B) \chi_2(C, D) = \langle N_{ABCD} \rangle. \quad (3)$$

In this Letter, we focus on demonstrating the power of the new fourfold cumulant mapping  $\chi_4$  by investigating the fragmentation of strong field ionized formaldehyde (undeuterated and deuterated). First, we show that this method can determine the relative, correlated momenta of all the ionic fragments produced by full Coulomb explosion of the molecule into atomic constituents. This is achieved at relatively high count rates and short data acquisition times,

essential for the extension of this technique to time-resolved measurements. Then, we show that a fourfold covariance analysis of the data is contaminated by the effect of pairwise correlations between the ions, which is eliminated by using the full cumulant formula. Finally, we use the method to contrast the Coulomb explosion dynamics of formaldehyde with 30- and 6-fs pulses. This shows that the fragmentation dynamics are more complex for the 30-fs case, in contrast to the 6-fs case, where the dynamics more closely match the expectation for a swift Coulomb repulsion following impulsive ionization of the molecule.

Our experiments make use of a velocity map imaging (VMI) apparatus [43] outfitted with a Tpx3Cam camera [44], illustrated in Fig. 1(a). The laser pulses originate from a commercial amplified Ti:sapphire laser system, which produces 30-fs laser pulses with 1 mJ of energy at a repetition rate of 1 kHz. The pulses are spectrally broadened in a stretched hollow core fiber (SHCF) [45–48] and compressed using chirped mirrors to a minimum duration of about 6 fs. The pulses (30 fs from the amplifier or 6 fs from the SHCF) are focused into our VMI apparatus.

The sample, deuterated or undeuterated formaldehyde, is obtained by sublimation of paraformaldehyde (purity 98%,

Sigma-Aldrich) at 50–60 °C. A skimmed molecular beam of sample molecules intersects the laser in the VMI apparatus.

The ionized fragments are accelerated toward the micro-channel plates (MCP) and phosphor screen under velocity-mapping condition. The fluorescence from hits on the phosphor screen is imaged onto the camera with an  $f/0.95$  lens. The 1-ns precision of the Tpx3Cam is sufficient to resolve the ion's momentum along the time-of-flight (TOF) direction, which can be used to reconstruct the full 3D-vector momenta of ions [7,44,49]. For the data presented here, the typical acquisition time was approximately 20 min, with on average eight ions detected per shot. The detection efficiency of our apparatus is estimated to be  $\eta = 60\%–90\%$  per particle, resulting in a fourfold channel overall efficiency of around  $\eta^4 = 13\%–65\%$  [41].

The full 3D information of correlated particles can be used to reconstruct the recoil frame and determine the kinetic energy release and angular distributions in the same way as coincidence measurements [7,37]. A description of the algorithm to compute the four-body cumulants is provided in Supplemental Material [50]. In our approach, the computational complexity has been simplified by introducing approximations such that we are able to compute them in a reasonable amount of time ( $\approx 1$  min). The detailed discussion on this technical point is discussed in a separate publication.

The recoil frame can be defined in the following way: The bisector of two  $\text{H}^+(\text{D}^+)$  unit momentum vectors defines the positive  $x$  axis, while the difference between the two  $\text{H}^+$  momenta unit vectors defines the positive  $y$  axis. The positive  $z$  axis can then be defined by computing the vector cross product of  $x$  and  $y$ . The definition is illustrated in Supplemental Fig. S1 [50]. Once the recoil frame is defined for each  $\text{H}^+$  pair, one can project the momenta of all four particles onto that frame. Figure 1(b) shows the correlated momentum distribution of all four particles in this frame. As can be seen from Fig. 1(b), the  $\text{O}^+$  is ejected preferentially along the negative  $x$  axis, which is opposite to the two  $\text{H}^+$ , while the  $\text{C}^+$  momentum is mostly along the positive  $x$  direction. Such a distribution bears a clear resemblance to the initial molecular geometry. A ball-and-stick model of the molecule is included in the figure to illustrate the fragmentation.

As a further test of the fourfold cumulant mapping method, we consider momentum conservation for four fragment ions. Figure 2 shows the comparison of the momentum sum along the lab frame  $x$  direction (laser polarization direction) of the four fragments using  $\chi_4$  or  $\kappa_4$ . Here, a deuterated sample was used to avoid counting  $\text{H}^+$  produced by background gases in the chamber. Because of momentum conservation in a full four-body breakup of the tetracation, we can see a sharp peak located at zero in both cases. The width of the distribution essentially reflects the momentum resolution of our detection apparatus.

For the curve depicting  $\chi_4$ , in addition to the narrow peak at zero, we see that there is a broad peak extending

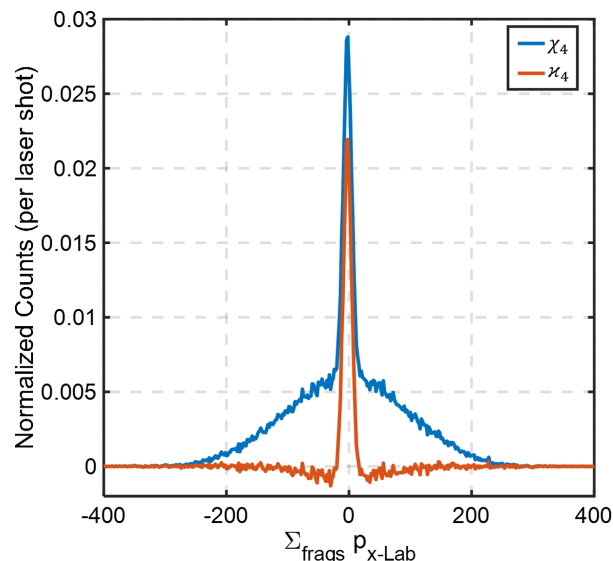


FIG. 2. Demonstration of momentum conservation along the lab frame laser polarization direction ( $x$ ) for four-body dissociation of quadruply ionized deuterated formaldehyde ( $\text{D}^+, \text{D}^+, \text{C}^+, \text{O}^+$ ) using 30-fs 240 TW/cm<sup>2</sup> laser pulses. Momentum units are  $\hbar/a_0$ . The blue curve shows a histogram using  $\chi_4$ , and the red curve represents  $\kappa_4$  [see Eqs. (2) and (3)].

over  $200\hbar/a_0$ . It arises from the product of two particle correlation terms:  $\Sigma\chi_2(N_1, N_2)\chi_2(N_3, N_4)$ . All fragment ion pairs contribute to this term, resulting in a roughly Gaussian-distributed background. This illustrates the importance of using the correction in calculating the appropriate four-particle correlation, which is equivalent to the calculation of a cumulant [41].

In contrast, the corrected correlation calculation,  $\kappa_4$ , yields an almost perfect delta function, despite some small negative values between  $\pm 100\hbar/a_0$ , which can arise from small fluctuations in the molecular density or laser intensity [34,39,51,52] or overlapping hits on the detector. Various techniques have been proposed to solve the fluctuation issue [38–40]. Further investigation is required in the context of a fourfold analysis. Note that the momentum conservation that we obtained here is not assumed or enforced by the algorithm, meaning that it comes out directly from the cumulant calculation. This is a strong indication that our approach isolates signals from the four-body fragmentation of interest. Further evidence can be found in the progression of correlation orders in the conventional TOF-TOF analysis, which is provided in Supplemental Material [50].

In order to highlight the ability of four-particle correlations to capture pulse shape or time-dependent structural changes, we compare the  $\text{O}^+$  distribution from covariant four-particle measurements (such as the one shown in Fig. 1) for 30- and 6-fs pulses. These results are shown in Fig. 3. Compared to the  $\text{O}^+$  from a 30-fs pulse, the yield from a 6-fs pulse has a significantly lower signal-to-noise ratio due to fewer counts, and it is more centered on the

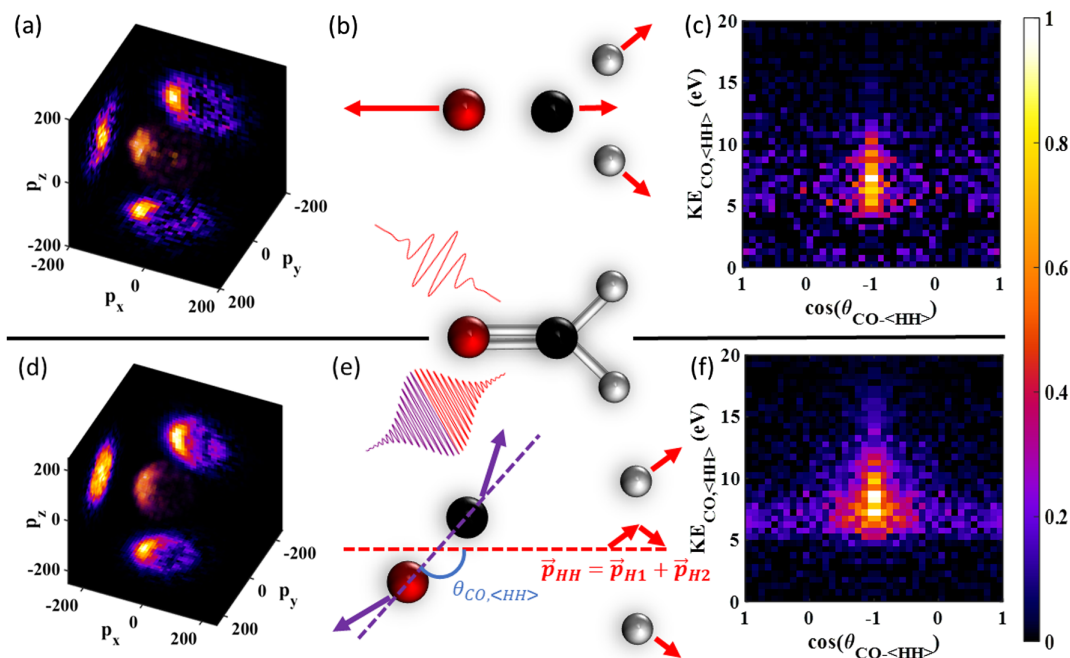


FIG. 3. Comparison of CEI with 6-fs 1300 TW/cm<sup>2</sup> pulses (top row) and 30-fs 240 TW/cm<sup>2</sup> pulses (bottom row) using fourfold cumulant imaging  $\chi_4(\text{H}^+, \text{H}^+, \text{C}^+, \text{O}^+)$ . (a) and (d) show 3D histograms of the  $\text{O}^+$  momentum distribution in the recoil frame, similar to Fig. 1. Momentum units are  $\hbar/a_0$ . (b) and (e) depict possible concerted and sequential breakup dynamics of the molecule for short (6-fs) or long (30-fs) pulses, respectively. The laser pulse and momentum vectors of the four fragments are also colored to indicate a possible time ordering of the breakup process. (c) and (f) show a native frame analysis of (a) and (d) by correlating the dissociation energy of the  $\text{CO}^{2+}$  fragment and the native frame angle ( $\text{CO}/\langle\text{HH}\rangle$ ), assuming the two  $\text{H}^+$  ions leave first. The angle axis is mirrored to put the main distribution in the center.

x axis. This observation is consistent with earlier coincidence measurements on the same molecule using 7-fs pulses [53]. The significantly higher yield and broader angle distribution for the 30-fs pulse as compared to the 6-fs pulse can be related to dynamics during the ionization processes. Enhanced ionization has been observed to increase the production of high-charge states in many small molecules, facilitated by dynamics on lower-charge states during the pulse [31,54–59].

Dynamics during ionization (e.g., rotation of the CO fragment after C–H dissociation) for the 30-fs pulses can also lead to broader angular distributions of the  $\text{O}^+$  fragment, as illustrated in Fig. 3. It is not clear from our measurements if the C–O dissociation takes place during the laser pulse, but it is clear that some rotation takes place after  $\text{H}^+$  dissociation but before dissociation is complete. Similar dynamics are considered in the coincidence imaging of the three-body channels ( $\text{H}^+, \text{H}^+, \text{CO}^+$ ) and ( $\text{H}^+, \text{CH}^+, \text{O}^+$ ) studied in earlier work [53].

Our single-pulse measurements cannot rule out other possibilities, such as sequential dissociation of ( $\langle\text{HH}\rangle, \text{CO}$ ) with subsequent rotation and dissociation of the CO. It has been demonstrated recently that a native frame analysis, making use of three-body Jacobi coordinates, can be very useful in separating sequential from concerted dynamics [40,60,61]. Briefly, in sequential dissociation, there is

competition between rotation and the second dissociation, resulting in a broad angular distribution for the fragments resulting from the second dissociation. The analysis is usually carried out for three-body problems, whereas there are four fragments in the present dissociation channel. Thus, we consider the dissociation of the two  $\text{H}^+$  as a single initial event, with their center of mass momentum represented by  $\langle\text{HH}\rangle$ , with the  $\text{OC}^{2+}$  breakup being a separate event, which can happen concertedly or sequentially, after the C–H dissociation. The native frame angles between  $\text{CO}^{2+}$  and  $\langle\text{HH}\rangle$ , as well as the dissociation energy of ( $\text{C}^+, \text{O}^+$ ), are shown in Fig. 3(e). In this frame, it is clear that between a dissociation energy of 5 and 8 eV, the 30-fs pulse measurements show a long tail outside the main peak at 180°, while 6-fs does not. A clear difference in the ionization dynamics for the two pulse durations is spotted, which suggests that the C–O dissociation takes place sequentially, after the C–H dissociation. The kinetic energy released into the ( $\text{C}^+, \text{O}^+$ ) pair is in good agreement with the  $\text{CO}^{2+}$  dissociation energy measured in earlier coincidence experiments with carbonyl sulfide (OCS) molecule [60], suggesting that the same metastable  $\text{CO}^{2+}$  intermediate is involved. A time-dependent (i.e., pump-probe) measurement would be required to reveal the full dissociation dynamics, for which high-count-rate covariance measurements are key.

In conclusion, we have demonstrated the experimental implementation of four-particle cumulant velocity map imaging, which can be used to track ultrafast structural dynamics in small molecules. We illustrate the importance of using the fourfold cumulant  $\chi_4$  over fourfold covariance  $\chi_4$  by confirming momentum conservation in the ( $D^+$ ,  $D^+$ ,  $C^+$ ,  $O^+$ ) channel. Our analysis highlights the ability to view the explosion dynamics in the recoil frame and demonstrates the sensitivity to ultrafast dynamics using high-fold cumulants. While the single-pulse measurements presented here do not provide a full picture of the dynamics in question, they motivate and enable time-resolved pump-probe measurements with cumulant analysis, which can be carried out with count rates about 2 orders of magnitude higher than coincidence measurements. We anticipate that cumulant mapping will be particularly valuable for analyzing the Coulomb explosion induced by XFELs, where the x-ray intensity is so high that coincidence analysis becomes overwhelmed by the event rate. Moreover, this analysis is not restricted to fourfold. Cumulants with even higher order are now accessible using the proposed algorithm.

F. A. acknowledges the EPSRC for their support. M. B. gratefully acknowledges support of the EPSRC (Program Grant No. EP/V026690/1). R. F. acknowledges support from the Linac Coherent Light Source, SLAC National Accelerator Laboratory, which is supported by the U.S. Department of Energy, Office of Science, Office of Basic Energy Sciences, under Contract No. DE-AC02-76SF00515. In addition, R. F., F. A., and P. H. B. were supported by the U.S. Department of Energy, Office of Science, Basic Energy Sciences, Chemical Sciences, Geosciences, and Biosciences Division, AMOS Program under SLAC FWP SCW0063. D. R. was supported by Contract No. DE-FG02-86ER13491 from the same agency. A. J. H. was supported by the National Science Foundation. A. J. H. was additionally supported under a Stanford Graduate Fellowship as the 2019 Albion Walter Hewlett Fellow. C. C., G. M., and T. W. acknowledge support from the U.S. Department of Energy under Grant No. DEFG02-08ER15984. The authors thank Taran Driver (SLAC National Accelerator Laboratory) for fruitful discussions and for helping to facilitate this research collaboration.

- 
- [1] J. Eland, Dynamics of fragmentation reactions from peak shapes in multiparticle coincidence experiments, *Laser Chem.* **11**, 259 (1991).
- [2] M. Lavollée and H. Bergeron, Data treatment in multiparticle coincidence experiments: Two-step dissociation processes, *J. Phys. B* **25**, 3101 (1992).
- [3] A. Landers, T. Weber, I. Ali, A. Cassimi, M. Hattass, O. Jagutzki, A. Nauert, T. Osipov, A. Staudte, M. Prior *et al.*, Photoelectron Diffraction Mapping: Molecules Illuminated from Within, *Phys. Rev. Lett.* **87**, 013002 (2001).

- [4] L. Holmegaard, J. L. Hansen, L. Kalhøj, S. Louise Kragh, H. Stapelfeldt, F. Filsinger, J. Küpper, G. Meijer, D. Dimitrovski, M. Abu-Samha *et al.*, Photoelectron angular distributions from strong-field ionization of oriented molecules, *Nat. Phys.* **6**, 428 (2010).
- [5] T. Jahnke, T. Weber, T. Osipov, A. Landers, O. Jagutzki, L. P. H. Schmidt, C. Cocke, M. Prior, H. Schmidt-Böcking, and R. Dörner, Multicoincidence studies of photo and Auger electrons from fixed-in-space molecules using the COLTRIMS technique, *J. Electron Spectrosc. Relat. Phenom.* **141**, 229 (2004).
- [6] A. Staudte, S. Patchkovskii, D. Pavičić, H. Akagi, O. Smirnova, D. Zeidler, M. Meckel, D. Villeneuve, R. Dörner, M. Y. Ivanov *et al.*, Angular Tunneling Ionization Probability of Fixed-in-Space  $H_2$  Molecules in Intense Laser Pulses, *Phys. Rev. Lett.* **102**, 033004 (2009).
- [7] F. Allum, C. Cheng, A. J. Howard, P. H. Bucksbaum, M. Brouard, T. Weinacht, and R. Forbes, Multi-particle three-dimensional covariance imaging: “Coincidence” insights into the many-body fragmentation of strong-field ionized  $D_2O$ , *J. Phys. Chem. Lett.* **12**, 8302 (2021).
- [8] F. Légaré, K. F. Lee, I. Litvinyuk, P. Dooley, S. Wesolowski, P. Bunker, P. Dombi, F. Krausz, A. Bandrauk, D. Villeneuve *et al.*, Laser Coulomb-explosion imaging of small molecules, *Phys. Rev. A* **71**, 013415 (2005).
- [9] M. Pitzer, M. Kunitski, A. S. Johnson, T. Jahnke, H. Sann, F. Sturm, L. P. H. Schmidt, H. Schmidt-Böcking, R. Dörner, J. Stohner *et al.*, Direct determination of absolute molecular stereochemistry in gas phase by Coulomb explosion imaging, *Science* **341**, 1096 (2013).
- [10] K. Fehre, S. Eckart, M. Kunitski, M. Pitzer, S. Zeller, C. Janke, D. Trabert, J. Rist, M. Weller, A. Hartung *et al.*, Enantioselective fragmentation of an achiral molecule in a strong laser field, *Sci. Adv.* **5**, eaau7923 (2019).
- [11] Y. Jiang, A. Rudenko, O. Herrwerth, L. Foucar, M. Kurka, K. Kühnel, M. Lezius, M. F. Kling, J. van Tilborg, A. Belkacem *et al.*, Ultrafast Extreme Ultraviolet Induced Isomerization of Acetylene Cations, *Phys. Rev. Lett.* **105**, 263002 (2010).
- [12] S. Bhattacharyya, K. Borne, F. Ziaee, S. Pathak, E. Wang, A. S. Venkatachalam, X. Li, N. Marshall, K. D. Carnes, C. W. Fehrenbach *et al.*, Strong-field-induced Coulomb explosion imaging of tribromomethane, *J. Phys. Chem. Lett.* **13**, 5845 (2022).
- [13] M. Burt, K. Amini, J. W. Lee, L. Christiansen, R. R. Johansen, Y. Kobayashi, J. D. Pickering, C. Vallance, M. Brouard, and H. Stapelfeldt, Communication: Gas-phase structural isomer identification by Coulomb explosion of aligned molecules, *J. Chem. Phys.* **148**, 091102 (2018).
- [14] I. Bocharova, A. Alnaser, U. Thumm, T. Niederhausen, D. Ray, C. L. Cocke, and I. Litvinyuk, Time-resolved Coulomb-explosion imaging of nuclear wave-packet dynamics induced in diatomic molecules by intense few-cycle laser pulses, *Phys. Rev. A* **83**, 013417 (2011).
- [15] S. De, M. Magrakvelidze, I. Bocharova, D. Ray, W. Cao, I. Znakovskaya, H. Li, Z. Wang, G. Laurent, U. Thumm *et al.*, Following dynamic nuclear wave packets in  $N_2$ ,  $O_2$ , and CO with few-cycle infrared pulses, *Phys. Rev. A* **84**, 043410 (2011).

- [16] F. Allum, M. Burt, K. Amini, R. Boll, H. Köckert, P. K. Olshin, S. Bari, C. Bomme, F. Brauße, B. Cunha de Miranda *et al.*, Coulomb explosion imaging of  $\text{CH}_3\text{I}$  and  $\text{CH}_2\text{ClI}$  photodissociation dynamics, *J. Chem. Phys.* **149**, 204313 (2018).
- [17] M. Burt, R. Boll, J. W. Lee, K. Amini, H. Köckert, C. Vallance, A. S. Gentleman, S. R. Mackenzie, S. Bari, C. Bomme *et al.*, Coulomb-explosion imaging of concurrent  $\text{CH}_2\text{BrI}$  photodissociation dynamics, *Phys. Rev. A* **96**, 043415 (2017).
- [18] X. Ding, R. Forbes, M. Kübel, K. F. Lee, M. Spanner, A. Y. Naumov, D. Villeneuve, A. Stolow, P. Corkum, and A. Staudte, Threshold photodissociation dynamics of  $\text{NO}_2$  studied by time-resolved cold target recoil ion momentum spectroscopy, *J. Chem. Phys.* **151**, 174301 (2019).
- [19] F. Allum, N. Anders, M. Brouard, P. Bucksbaum, M. Burt, B. Downes-Ward, S. Grundmann, J. Harries, Y. Ishimura, H. Iwayama *et al.*, Multi-channel photodissociation and XUV-induced charge transfer dynamics in strong-field-ionized methyl iodide studied with time-resolved recoil-frame covariance imaging, *Faraday Discuss.* **228**, 571 (2021).
- [20] A. J. Howard, M. Britton, Z. L. Streeter, C. Cheng, R. Forbes, J. L. Reynolds, F. Allum, G. A. McCracken, I. Gabalski, R. R. Lucchese, C. W. McCurdy, T. Weinacht, and P. H. Bucksbaum, Filming enhanced ionization in an ultrafast triatomic slingshot, [arXiv:2210.13645](https://arxiv.org/abs/2210.13645).
- [21] D. M. Bittner, K. Gope, and D. Strasser, Time-resolved dissociative ionization and double photoionization of  $\text{CO}_2$ , *J. Chem. Phys.* **153**, 194201 (2020).
- [22] T. Endo, S. P. Neville, V. Wanie, S. Beaulieu, C. Qu, J. Deschamps, P. Lassonde, B. E. Schmidt, H. Fujise, M. Fushitani *et al.*, Capturing roaming molecular fragments in real time, *Science* **370**, 1072 (2020).
- [23] E. Wang, X. Shan, L. Chen, T. Pfeifer, X. Chen, X. Ren, and A. Dorn, Ultrafast proton transfer dynamics on the repulsive potential of the ethanol dication: Roaming-mediated isomerization versus Coulomb explosion, *J. Phys. Chem. A* **124**, 2785 (2020).
- [24] N. Ekanayake, T. Severt, M. Nairat, N. P. Weingartz, B. M. Farris, B. Kaderiya, P. Feizollah, B. Jochim, F. Ziaee, K. Borne *et al.*,  $\text{H}_2$  roaming chemistry and the formation of  $\text{H}_3^+$  from organic molecules in strong laser fields, *Nat. Commun.* **9**, 1 (2018).
- [25] E. Livshits, I. Luzon, K. Gope, R. Baer, and D. Strasser, Time-resolving the ultrafast  $\text{H}_2$  roaming chemistry and  $\text{H}_3^+$  formation using extreme-ultraviolet pulses, *Commun. Chem. B* **3**, 1 (2020).
- [26] K. Gope, E. Livshits, D. M. Bittner, R. Baer, and D. Strasser, Two pathways and an isotope effect in  $\text{H}_3^+$  formation following double ionization of methanol, *Nat. sci.* **1**, e10022 (2021).
- [27] I. Luzon, E. Livshits, K. Gope, R. Baer, and D. Strasser, Making sense of Coulomb explosion imaging, *J. Phys. Chem. Lett.* **10**, 1361 (2019).
- [28] K. Gope, I. Luzon, and D. Strasser, N–NO & NN–O bond cleavage dynamics in two- and three-body Coulomb explosion of the  $\text{N}_2\text{O}_2^+$  dication, *Phys. Chem. Chem. Phys.* **21**, 13730 (2019).
- [29] R. Boll, J. M. Schäfer, B. Richard, K. Fehre, G. Kastirke, Z. Jurek, M. S. Schöffler, M. M. Abdullah, N. Anders, T. M. Baumann *et al.*, X-ray multiphoton-induced Coulomb explosion images complex single molecules, *Nat. Phys.* **18**, 423 (2022).
- [30] X. Li, A. Rudenko, M. Schöffler, N. Anders, T. M. Baumann, S. Eckart, B. Erk, A. De Fanis, K. Fehre, R. Dörner *et al.*, Coulomb explosion imaging of small polyatomic molecules with ultrashort x-ray pulses, *Phys. Rev. Res.* **4**, 013029 (2022).
- [31] A. Howard, C. Cheng, R. Forbes, G. McCracken, W. Mills, V. Makhija, M. Spanner, T. Weinacht, and P. Bucksbaum, Strong-field ionization of water: Nuclear dynamics revealed by varying the pulse duration, *Phys. Rev. A* **103**, 043120 (2021).
- [32] L. Frasinski, K. Codling, and P. Hatherly, Covariance mapping: A correlation method applied to multiphoton multiple ionization, *Science* **246**, 1029 (1989).
- [33] I. Noda, Generalized two-dimensional correlation method applicable to infrared, Raman, and other types of spectroscopy, *Appl. Spectrosc.* **47**, 1329 (1993).
- [34] L. J. Frasinski, Covariance mapping techniques, *J. Phys. B* **49**, 152004 (2016).
- [35] J. D. Pickering, K. Amini, M. Brouard, M. Burt, I. J. Bush, L. Christensen, A. Lauer, J. H. Nielsen, C. S. Slater, and H. Stapelfeldt, Communication: Three-fold covariance imaging of laser-induced Coulomb explosions, *J. Chem. Phys.* **144**, 161105 (2016).
- [36] C. S. Slater, S. Blake, M. Brouard, A. Lauer, C. Vallance, J. J. John, R. Turchetta, A. Nomerotski, L. Christensen, J. H. Nielsen *et al.*, Covariance imaging experiments using a pixel-imaging mass-spectrometry camera, *Phys. Rev. A* **89**, 011401(R) (2014).
- [37] J. W. Lee, H. Köckert, D. Heathcote, D. Popat, R. T. Chapman, G. Karras, P. Majchrzak, E. Springate, and C. Vallance, Three-dimensional covariance-map imaging of molecular structure and dynamics on the ultrafast timescale, *Commun. Chem. B* **3**, 1 (2020).
- [38] L. Frasinski, V. Zhaunerchyk, M. Mücke, R. J. Squibb, M. Siano, J. H. D. Eland, P. Linusson, P. Vd Meulen, P. Salén, R. Thomas *et al.*, Dynamics of Hollow Atom Formation in Intense X-Ray Pulses Probed by Partial Covariance Mapping, *Phys. Rev. Lett.* **111**, 073002 (2013).
- [39] V. Zhaunerchyk, L. Frasinski, J. H. D. Eland, and R. Feifel, Theory and simulations of covariance mapping in multiple dimensions for data analysis in high-event-rate experiments, *Phys. Rev. A* **89**, 053418 (2014).
- [40] J. W. McManus, T. Walmsley, K. Nagaya, J. R. Harries, Y. Kumagai, H. Iwayama, M. N. Ashfold, M. Britton, P. H. Bucksbaum, B. Downes-Ward *et al.*, Disentangling sequential and concerted fragmentations of molecular polycations with covariant native frame analysis, *Phys. Chem. Chem. Phys.* **24**, 22699 (2022).
- [41] L. J. Frasinski, Cumulant mapping as the basis of multi-dimensional spectrometry, *Phys. Chem. Chem. Phys.* **24**, 20776 (2022).
- [42] Either by symmetry or via the use of a moment generation function.
- [43] A. T. Eppink and D. H. Parker, Velocity map imaging of ions and electrons using electrostatic lenses: Application in photoelectron and photofragment ion imaging of molecular oxygen, *Rev. Sci. Instrum.* **68**, 3477 (1997).

- [44] A. Zhao, M. van Beuzekom, B. Bouwens, D. Byelov, I. Chakaberia, C. Cheng, E. Maddox, A. Nomerotski, P. Svihra, J. Visser *et al.*, Coincidence velocity map imaging using Tpx3Cam, a time stamping optical camera with 1.5 ns timing resolution, *Rev. Sci. Instrum.* **88**, 113104 (2017).
- [45] A. Catanese, B. Kaufman, C. Cheng, E. Jones, M. G. Cohen, and T. Weinacht, Acousto-optic modulator pulse-shaper compression of octave-spanning pulses from a stretched hollow-core fiber, *OSA Continuum* **4**, 3176 (2021).
- [46] M. Nisoli, S. De Silvestri, and O. Svelto, Generation of high energy 10 fs pulses by a new pulse compression technique, *Appl. Phys. Lett.* **68**, 2793 (1996).
- [47] T. Nagy, P. Simon, and L. Veisz, High-energy few-cycle pulses: Post-compression techniques, *Adv. Phys. X* **6**, 1845795 (2021).
- [48] T. Nagy, M. Forster, and P. Simon, Flexible hollow fiber for pulse compressors, *Appl. Opt.* **47**, 3264 (2008).
- [49] C. Cheng, R. Forbes, A. J. Howard, M. Spanner, P. H. Bucksbaum, and T. Weinacht, Momentum-resolved above-threshold ionization of deuterated water, *Phys. Rev. A* **102**, 052813 (2020).
- [50] See Supplemental Material at <http://link.aps.org/supplemental/10.1103/PhysRevLett.130.093001> for detailed algorithms computing the fourfold cumulant mapping and additional analysis.
- [51] J. Mikosch and S. Patchkovskii, Coincidence and covariance data acquisition in photoelectron and-ion spectroscopy. I. Formal theory, *J. Mod. Opt.* **60**, 1426 (2013).
- [52] J. Mikosch and S. Patchkovskii, Coincidence and covariance data acquisition in photoelectron and-ion spectroscopy. II. Analysis and applications, *J. Mod. Opt.* **60**, 1439 (2013).
- [53] C.-M. Tseng, M. Fushitani, A. Matsuda, and A. Hishikawa, Coincidence momentum imaging of four- and three-body Coulomb explosion of formaldehyde in ultrashort intense laser fields, *J. Electron Spectrosc. Relat. Phenom.* **228**, 25 (2018).
- [54] C. Cheng, Z. L. Streeter, A. J. Howard, M. Spanner, R. R. Lucchese, C. W. McCurdy, T. Weinacht, P. H. Bucksbaum, and R. Forbes, Strong-field ionization of water. II. Electronic and nuclear dynamics en route to double ionization, *Phys. Rev. A* **104**, 023108 (2021).
- [55] T. Seideman, M. Y. Ivanov, and P. B. Corkum, Role of Electron Localization in Intense-Field Molecular Ionization, *Phys. Rev. Lett.* **75**, 2819 (1995).
- [56] I. Bocharova, R. Karimi, E. F. Penka, J.-P. Brichta, P. Lassonde, X. Fu, J.-C. Kieffer, A. D. Bandrauk, I. Litvinyuk, J. Sanderson *et al.*, Charge Resonance Enhanced Ionization of CO<sub>2</sub> Probed by Laser Coulomb Explosion Imaging, *Phys. Rev. Lett.* **107**, 063201 (2011).
- [57] H. Liu, M. Li, X.-G. Xie, C. Wu, Y.-K. Deng, C.-Y. Wu, Q.-H. Gong, and Y.-Q. Liu, Charge resonance enhanced multiple ionization of H<sub>2</sub>O molecules in intense laser fields, *Chin. Phys. Lett.* **32**, 063301 (2015).
- [58] F. L egar e, I. Litvinyuk, P. Dooley, F. Qu er e, A. Bandrauk, D. Villeneuve, and P. Corkum, Time-Resolved Double Ionization with Few Cycle Laser Pulses, *Phys. Rev. Lett.* **91**, 093002 (2003).
- [59] S. Koh, K. Yamazaki, M. Kanno, H. Kono, and K. Yamanouchi, Ionization and dissociation dynamics of H<sub>2</sub>O in ultrashort intense near-IR laser fields by the time-dependent adiabatic state method and the time-dependent configuration interaction method, *Chem. Phys. Lett.* **742**, 137165 (2020).
- [60] J. Rajput, T. Severt, B. Berry, B. Jochim, P. Feizollah, B. Kaderiya, M. Zohrabi, U. Ablikim, F. Ziaee, D. Rolles *et al.*, Native Frames: Disentangling Sequential from Concerted Three-Body Fragmentation, *Phys. Rev. Lett.* **120**, 103001 (2018).
- [61] T. Severt, Z. L. Streeter, W. Iskandar, K. A. Larsen, A. Gatton, D. Trabert, B. Jochim, B. Griffin, E. G. Champenois, M. M. Brister *et al.*, Step-by-step state-selective tracking of fragmentation dynamics of water dications by momentum imaging, *Nat. Commun.* **13**, 5146 (2022).